International Journal of Applied Mathematics and Theoretical Physics
2026, Vol. 12, No. 3, pp. 79–93
https://doi.org/10.11648/j.ijamtp.20261203.11

Research Article

Parametric Assessment of Thermal Energy Transport in Magnetohydrodynamic Silver Nanofluid Flow over a Cylindrical Geometry

Ojo Adetoye Solomon[1,*], Nwabuzor Peter Onyelukachukwu[2]

[1]Department of Physics, University of Port Harcourt, Port Harcourt, Nigeria

[2]Department of Physics with Electronics, University of Port Harcourt, Port Harcourt, Nigeria

Abstract

Thermal energy transport remains a critical challenge in engineering systems, particularly in applications involving advanced cooling technologies, chemical processing, energy conversion, and thermal management devices. This study presents a parametric assessment of thermal energy transport in magnetohydrodynamic (MHD) silver nanofluid flow over a cylindrical geometry by examining the influence of key thermo-physical and flow parameters on heat and mass transfer characteristics. To accurately predict the effective properties of the nanofluid, hybrid constitutive models were adopted by combining the thermal conductivity correlations of Jang and Choi (2004) and Xue (2005), together with the viscosity models of Mooney (1951) and Saito (1950). These models account for the effects of nanoparticle concentration, particle size, temperature, and particle geometry on the transport properties of the nanofluid. The mathematical formulation consists of the continuity, momentum, energy, and concentration equations expressed in cylindrical coordinates. The governing equations incorporate magnetohydrodynamic effects and thermal radiation through the Rosseland diffusion approximation. Analytical solutions were obtained using the Laplace transform technique and evaluated with Wolfram Mathematica Version 12. The influence of the governing dimensionless parameters on the velocity, temperature, and concentration distributions, together with the engineering performance indices including skin friction coefficient, Nusselt number, and Sherwood number, was systematically investigated. The results reveal that increasing the Prandtl number significantly suppresses the thermal boundary layer, leading to a reduction in the nanofluid temperature profile. A similar decline in temperature is observed with increasing thermal radiation parameter, indicating enhanced thermal energy dissipation. Furthermore, variations in the Grashof number, Reynolds number, Schmidt number, and chemical reaction parameter substantially influence the momentum, thermal, and concentration boundary layers. The combined thermo-physical models provide improved prediction of transport behaviour and demonstrate the potential of silver nanofluids for enhanced thermal performance in engineering systems involving cylindrical geometries under magnetic field effects.

Keywords

Silver Nanofluid, Magnetohydrodynamic (MHD) Flow, Thermal Energy Transport, Cylindrical Geometry, Laplace Transform

*Correspondence: Ojo Adetoye Solomon (solomontoye10@gmail.com)

Received: 22 July 2026; **Accepted:** 30 July 2026; **Published:** 20 August 2026

1. Introduction

Thermal energy transport plays a fundamental role in the performance and efficiency of numerous engineering systems, including heat exchangers, chemical reactors, electronic cooling devices, energy conversion units, and metallurgical processes. The increasing demand for high-performance thermal management has stimulated extensive research into techniques for enhancing heat transfer through the modification of flow configurations, boundary conditions, and the thermophysical properties of working fluids. Among these approaches, nanofluids have emerged as promising heat transfer media due to their superior thermal conductivity and enhanced transport characteristics compared with conventional fluids. In particular, silver (Ag) nanofluids have attracted considerable attention because of their excellent thermal conductivity, making them suitable for applications requiring efficient thermal energy transport.

Magnetohydrodynamics (MHD), which describes the interaction between electrically conducting fluids and externally applied magnetic fields, has become an important area of research in engineering physics. Conducting fluids such as liquid metals, molten salts, plasmas, electrolytes, and nanofluids exhibit altered flow behaviour when subjected to magnetic fields. The induced Lorentz force modifies the fluid motion, influences the thermal and concentration boundary layers, and consequently affects heat and mass transfer characteristics [1]. The ability to manipulate fluid flow using magnetic fields has led to numerous engineering applications, including electromagnetic casting, liquid-metal cooling systems, induction furnaces, crystal growth, metallurgical processing, and nuclear reactor technologies, where precise control of heat transfer is essential [2].

The regulation of heat and mass transfer through magnetic field effects remains one of the major challenges in chemical and thermal engineering. Appropriate control of magnetic field intensity can either enhance or suppress convective heat transfer depending on the operating conditions and fluid properties. Previous investigations have demonstrated that variations in magnetic field strength significantly influence fluid velocity, temperature distribution, and heat transfer rates, thereby affecting the overall thermal performance of engineering systems [3]. The efficiency of convective heat transfer is commonly quantified using the Nusselt number, which represents the ratio of convective to conductive heat transfer and serves as a key performance indicator in thermal engineering.

Boundary-layer development also plays a significant role in determining thermal transport behaviour. The characteristic length of a flow domain together with the thermal conductivity of the working fluid governs the growth of the thermal boundary layer. Depending on the engineering configuration, the characteristic length may correspond to the diameter of a sphere, the length of a vertical plate, or the external diameter of a cylinder. For complex geometries, it is commonly evaluated as the ratio of the body's volume to its surface area [4]. Experimental and numerical investigations have further shown that increasing fluid velocity and buoyancy forces enhances the Nusselt number, thereby improving convective heat transfer in mixed-convection systems [5]. Similarly, increases in the magnetic parameter and Prandtl number have been reported to enhance local heat transfer in non-isothermal wedge flows under appropriate operating conditions [6].

Recent developments in nanofluid technology have further demonstrated that nanoparticle size, interfacial layer thickness, particle concentration, and rheological behaviour significantly affect thermal transport characteristics. Studies on non-Newtonian Jeffrey nanofluids flowing over curved stretching surfaces revealed that both nanoparticle diameter and liquid-solid interfacial layer dynamics substantially influence heat transfer enhancement [7]. Likewise, hybrid analytical techniques have been successfully employed to investigate MHD flow and heat transfer in temperature-dependent viscous fluids, providing valuable insight into the corresponding skin friction characteristics and wall shear behaviour [8]. High-fidelity numerical simulations have also demonstrated that increasing Reynolds and Prandtl numbers modifies turbulent structures and alters heat transfer within channel flows [9]. In biomedical engineering applications, investigations of MHD micropolar fluid flow through bifurcated arteries have shown that buoyancy effects, magnetic field strength, and heat source parameters strongly influence fluid motion and thermal transport [10].

The combined effects of chemical reactions, thermal radiation, and porous media have also attracted considerable attention in recent years. Investigations involving chemically reacting micropolar fluids have shown that chemical reactions and solute stratification significantly influence concentration boundary layers and mass transfer characteristics [11]. Similarly, studies on radiative MHD Poiseuille flow through porous media have demonstrated that radiation and porous structures substantially affect flow stability and thermal transport behaviour [12]. Stability analyses of exothermic reactions within porous media further indicate that nonlinear energy generation mechanisms strongly influence thermal stability, requiring multidimensional analysis for accurate prediction [13].

Numerous investigations have examined MHD heat transfer in enclosed and cylindrical geometries. Mixed convection studies in inclined enclosures have shown that the average Nusselt number generally increases with Reynolds number and enclosure inclination, whereas the influence of the Prandtl number is comparatively weaker under certain operating conditions [14]. Differential quadrature analyses of buoyancy-driven flows under transverse magnetic fields have further demonstrated that stronger magnetic fields tend to suppress convective heat transfer while increasing thermal diffusion [15]. Numerical studies of transient thermal convection have similarly reported that the Prandtl number significantly affects transient heat transfer behaviour [16]. Correlations developed for natural convection in enclosed geometries have further improved the prediction of engineering heat transfer processes [17].

Research on cylindrical geometries has become increasingly important because of their widespread application in heat exchangers, pipelines, cooling channels, and nuclear engineering. Previous investigations involving liquid-metal natural convection between concentric cylinders have shown that magnetic field intensity strongly influences the Nusselt number and overall heat transfer characteristics [18]. Direct numerical simulations have further revealed that the interaction between magnetic fields and buoyancy forces determines the transition between laminar and turbulent flow while generating Hartmann layers and three-dimensional flow structures [19, 20]. Additional numerical studies have demonstrated that increasing the Rayleigh number enhances convective heat transfer, whereas stronger magnetic fields promote conduction-dominated transport and reduce the average Nusselt number, particularly under vertically applied magnetic fields [21]. Similar observations have been reported for mixed convection over vertical cylinders, where magnetic field strength, Prandtl number, and Schmidt number significantly influence thermal and concentration boundary layers [22, 23].

Despite these important contributions, relatively few studies have investigated the combined influence of hybrid effective thermal conductivity and effective viscosity models on thermal energy transport in magnetohydrodynamic silver nanofluid flow over cylindrical geometries. Furthermore, the coupled effects of thermal radiation and transport properties on engineering performance indices, including skin friction coefficient, Nusselt number, and Sherwood number, remain insufficiently understood. Therefore, the present study performs a parametric assessment of thermal energy transport in magnetohydrodynamic silver nanofluid flow over a cylindrical geometry by integrating the effective thermal conductivity models of Jang and Choi (2004) and Xue (2005) with the viscosity models of Mooney (1951) and Saito (1950). The governing continuity, momentum, energy, and concentration equations are formulated in cylindrical coordinates and solved analytically using the Laplace transform technique while incorporating thermal radiation through the Rosseland diffusion approximation. The effects of the governing dimensionless parameters on the velocity, temperature, concentration, skin friction coefficient, Nusselt number, and Sherwood number are systematically investigated to provide valuable insight into the design and optimization of advanced thermal management systems employing electrically conducting silver nanofluids.

2. Mathematical Formulation of the Problem

The mathematical model governing the magnetohydrodynamic (MHD) flow and thermal energy transport of a silver nanofluid over a cylindrical geometry is formulated in the cylindrical coordinate system (r, z). The model is based on the conservation principles of mass, momentum, thermal energy, and species concentration. The governing equations incorporate the effects of an externally applied magnetic field, thermal radiation, chemical reaction, and the effective thermo-physical properties of the silver nanofluid.

$$\frac{1}{r}\frac{\partial}{\partial r}\left(\rho_{nf} r v_r\right)+\frac{\partial}{\partial t}\rho_{nf}=0 \tag{1}$$

$$\rho\left(\frac{\partial v_r}{\partial t}+v_r\frac{\partial v_r}{\partial r}\right)+-\frac{\partial \rho}{\partial r}=+\mu\left[\frac{\partial}{\partial r}\left(\frac{1}{r}\frac{\partial}{\partial r}(r v_r)\right)\right]+g\beta_C(C-C_0)+g\beta_T(T-T_0)-\left[\sigma B_0^2 v_r+\frac{\sigma_0}{v_r}\right] \tag{2}$$

$$\left(\rho\hat{C}_p\right)\left(\frac{\partial}{\partial t}T+v_r\frac{\partial}{\partial r}T\right)+\frac{1}{r}\frac{\partial}{\partial r}(r q_r)=K\left[\frac{1}{r}\frac{\partial}{\partial r}\left(r\frac{\partial}{\partial r}T\right)\right] \tag{3}$$

$$\left(\rho\hat{C}_p\right)\left(\frac{\partial}{\partial t}C+v_r\frac{\partial}{\partial r}C\right)+\frac{1}{r}\frac{\partial}{\partial r}(k_0 C)=K\left[\frac{1}{r}\frac{\partial}{\partial r}\left(r\frac{\partial C}{\partial r}\right)\right] \tag{4}$$

Substituting the effective thermo-physical properties of the silver nanofluid into Eqs. (5) - (8) yields the following governing equations:

$$\frac{1}{r}\frac{\partial}{\partial r}\left(\rho_{nf} r v_r\right)+\frac{\partial \rho_{nf}}{\partial t}=0 \tag{5}$$

$$\rho_{nf}\left(\frac{\partial v_r}{\partial t}+v_r\frac{\partial v_r}{\partial r}\right)=-\frac{\partial \rho}{\partial r}+\mu_{nf}\left[\frac{\partial}{\partial r}\left(\frac{1}{r}\frac{\partial}{\partial r}(r v_r)\right)\right]+g\beta_T(T-T_0)+g\beta_C(C-C_0)-\sigma B_0^2 v_r-\frac{\sigma_0}{v_r} \tag{6}$$

$$\left(\rho\hat{C}_p\right)_{nf}\left(\frac{\partial T}{\partial t}+v_r\frac{\partial T}{\partial r}\right)=K_{nf}\left[\frac{1}{r}\frac{\partial}{\partial r}\left(r\frac{\partial T}{\partial r}\right)\right]-\frac{1}{r}\frac{\partial}{\partial r}\left(rq_r\right) \tag{7}$$

$$\left(\rho\hat{C}_p\right)_{nf}\left(\frac{\partial C}{\partial t}+v_r\frac{\partial C}{\partial r}\right)=K_{nf}\left[\frac{1}{r}\frac{\partial}{\partial r}\left(r\frac{\partial C}{\partial r}\right)\right]-\frac{1}{r}\frac{\partial}{\partial r}\left(k_0 C\right) \tag{8}$$

Here, B_0 is uniform magnetic field strength, σ is electrical conductivity, K_{nf} is thermal conductivity of nanofluid, v_r is velocity fluid component, ρ_{nf} is fluid density of nanofluid, μ_{nf} is viscosity of nanofluid, β_{nf} is thermal expansion of nanofluid, T is temperature of nanofluid, C_p is specific heat at constant pressure, q_r is radiation term, k_0 is chemical reaction term, D is chemical molecular diffusivity, r is radius of nanoparticles.

Equations (5), (6), (7) and (8) can be rewritten respectively as

$$\frac{\partial\rho_{nf}}{\partial t}=-\frac{1}{r}\frac{\partial}{\partial r}\left(\rho_{nf}rv_r\right) \tag{9}$$

$$\frac{\partial v_r}{\partial t}+v_r\frac{\partial v_r}{\partial r}=\frac{\mu_{nf}}{\rho_{nf}}\left[\frac{\partial}{\partial r}\left(\frac{1}{r}\frac{\partial}{\partial r}(rv_r)\right)\right]-\frac{\sigma B_0{}^2 v_r}{\rho_{nf}}+\frac{g\beta_T(T-T_0)}{v_r^2}+\frac{g\beta_C(C-C_0)}{v_r^2}-\frac{\sigma_0}{v_r} \tag{10}$$

$$\frac{\partial T}{\partial t}+v_r\frac{\partial T}{\partial r}=\frac{K_{nf}}{\left(\rho\hat{C}_p\right)_{nf}}\left[\frac{1}{r}\frac{\partial}{\partial r}\left(r\frac{\partial T}{\partial r}\right)\right]-\frac{1}{\left(\rho\hat{C}_p\right)_{nf}}\frac{1}{r}\frac{\partial}{\partial r}\left(rq_r\right) \tag{11}$$

$$\frac{\partial C}{\partial t}+v_r\frac{\partial C}{\partial r}=\frac{D}{\left(\rho C_p\right)}\left[\frac{1}{r}\frac{\partial}{\partial r}\left(r\frac{\partial C}{\partial r}\right)\right]+\frac{1}{(\rho C_p)}\frac{1}{r}(k_0 C) \tag{12}$$

If the fluid is incompressible, then equation (9) results in

$$v_r=\frac{\rho}{r} \tag{13}$$

For an incompressible fluid, the density is assumed constant, and Equation (13) satisfies the continuity equation. Under steady-state conditions, the radial velocity obtained from Equation (13) is substituted into the momentum, energy, and concentration equations, resulting in the reduced governing Equations (14) - (16).

$$\frac{1}{r}\frac{\partial v_r}{\partial r}=\frac{\mu_{nf}}{\rho_{nf}}\left[\frac{1}{r}\frac{\partial v_r}{\partial r}+\frac{\partial^2 v_r}{\partial r^2}\right]-\frac{\sigma B_0{}^2 v_r}{\rho_{nf}}+\frac{g\beta_T(T-T_0)}{v_r^2}+\frac{g\beta_C(C-C_0)}{v_r^2}-\frac{\sigma_0}{v_r} \tag{14}$$

$$\frac{1}{r}\frac{\partial T}{\partial r}=\frac{K_{nf}}{\left(\rho\hat{C}_p\right)_{nf}}\left[\frac{1}{r}\frac{\partial T}{\partial r}+\frac{\partial T^2}{\partial r^2}\right]-\frac{1}{\left(\rho\hat{C}_p\right)_{nf}}\frac{1}{r}\frac{\partial}{\partial r}\left(rq_r\right) \tag{15}$$

$$\frac{1}{r}\frac{\partial C}{\partial r}=\frac{D}{\left(\rho C_p\right)}\left[\frac{1}{r}\frac{\partial C}{\partial r}+\frac{\partial C^2}{\partial r^2}\right]+\frac{1}{(\rho C_p)}\frac{1}{r}(k_0 C) \tag{16}$$

The governing equations are solved subject to the following boundary conditions:

$$v_r(0,t)=0, v_r(d,t)=u.T(0,t)=1, T(\infty,0)=0, C(0,t)=1, C(\infty,t)=0$$

(Ngiangia and Orukari [24])

To account for thermal radiation, the Rosseland diffusion approximation is employed under the assumption of an optically thick medium. Accordingly, the radiative heat flux is expressed as [25]:

$$\frac{\partial q_r}{\partial r} = -\frac{4K_B}{3\alpha}\frac{\partial T^4}{\partial r} \tag{17}$$

where α denotes the absorption coefficient and K_B stands for the Stefan-Boltzmann constant. If the temperature gradient within the nanofluid flow is so tiny that T^4 is a linear function of temperature, then. To do this, we extend T^4 in a Taylor series around T_∞ and exclude terms of higher order; this leads to the following expression:

$$T^4 = 4T_\infty^3 T - 3T_\infty^4 \tag{18}$$

Assuming sufficiently small temperature differences within the flow field, the term T^4 is expanded using a first-order Taylor series about the ambient temperature T_∞, while higher-order terms are neglected. Consequently,

$$\frac{\rho}{r}\frac{\partial T}{\partial r} = \frac{K_{nf}}{\left(\rho\hat{C}_p\right)_{nf}}\left(1+\frac{16K_0T^3}{3\alpha}\right)\frac{1}{r}\frac{\partial}{\partial r}\left(r\frac{\partial T}{\partial r}\right) - \frac{K_{nf}}{\left(\rho\hat{C}_p\right)_{nf}}\frac{1}{r}q_r \tag{19}$$

To improve the prediction of the effective thermal conductivity of the silver nanofluid, the thermal conductivity models proposed by Jang and Choi [26] and Xue [27] are combined. The resulting formulation accounts for Brownian motion, particle size, nanoparticle concentration, temperature, and particle geometry, thereby providing a more realistic representation of thermal energy transport in cylindrical and non-cylindrical nanoparticles.

$$K_{eff_1} = K_{bf}(1-\phi) + K_{np}\phi + 3C\frac{d_{bf}}{d_{np}}K_{bf}\,\mathrm{Re}_{d_{np}}^2\,\mathrm{Pr}\,\phi \tag{20}$$

$$K_{eff_2} = K_{bf}\frac{1-\phi+2\phi\dfrac{K_{np}}{K_{np}-K_{bf}}In\dfrac{K_{np}+K_{bf}}{2K_{bf}}}{1-\phi+2\phi\dfrac{K_{bf}}{K_{np}-K_{bf}}In\dfrac{K_{np}+K_{bf}}{2K_{bf}}} \tag{21}$$

Similarly, the effective viscosity employed in the momentum equation is obtained by combining the viscosity correlations proposed by Mooney [28] and Saito [29]. This combined formulation improves the prediction of flow behaviour, wall shear stress, pressure distribution, and temperature gradients within the silver nanofluid.

$$\mu_{eff_1} = \left\{1+2.5\phi_{np}+\left[3.125+\left(2.5/\phi_{np\max}\right)\right]\phi_{np}^2+....\right\}\mu_{bf} \tag{22}$$

$$\mu_{eff_2} = +\left(1+2.5\phi_{np}+2.5\phi_{np}^2+....\right)\mu_{bf} \tag{23}$$

From the work of [30], density of nanofluid (ρ_{nf}), thermal expansion due to temperature of nanofluid (β_{nf}), thermal expansion due to concentration of nanofluid (β_{nf}^*), specific heat at constant pressure of nanofluid $(C_p)_{nf}$, nanoparticle volume fraction (ϕ_{np}) are respectively stated as

$$\frac{\rho_{nf}}{\rho_{bf}} = (1-\phi)\rho_f + \phi\frac{\rho_{np}}{\rho_{bf}}$$

$$\frac{\beta_{nf}}{\beta_{bf}} = (1-\phi)\beta_f + \phi\frac{\beta_{np}}{\beta_{bf}} \tag{24}$$

$$\frac{\beta_{nf}^*}{\beta_{bf}} = (1-\phi)\beta_f^* + \phi\frac{\beta_{np}^*}{\beta_{bf}} \quad \frac{\left(C_p\right)_{nf}}{\left(C_p\right)_{bf}} = (1-\phi)\left(C_p\right)_f + \phi\frac{\left(C_p\right)_{np}}{\left(C_p\right)_{bf}}$$

Table 1. *Thermophysical properties of the selected individual nanofluids.*

Nanoparticles	$\rho(kgm^{-3})$	$\mu(kgm^{-1}s^{-1})$	k (W/mK)	$C_p(J^{-1}kgK)$
Silver (Ag)	10500	1.89×10^{-5}	429	235.0
Copper (Cu)	8933	1.67×10^{-5}	401	385
Tin Oxide (SnO_2)	6950	3.5×10^{-3}	8.95	686.2
Aluminium oxide (Al_2O_3)	3970	0.8×10^{-5}	40	765
Titanium dioxide (TiO_2)	4250	0.90×10^{-5}	8.9538	686.2

Nanoparticles	$\rho(kgm^{-3})$	$\mu(kgm^{-1}s^{-1})$	k (W/mK)	$C_\rho(J^{-1}kgK)$
Water	997	1.3×10^{-3}	0.613	4200
Ethylene Glycol	1082	4.8×10^{-3}	0.253	3140

3. Dimensional Analysis

To simplify the governing equations and facilitate the parametric investigation, the following dimensionless variables are introduced. By applying these transformations to Equations (14) - (16), the governing equations are expressed in nondimensional form as Equations (25) - (27).

$$\mathrm{Re}^{-1}=\frac{\mu_{nf}\rho_f}{\rho_{nf}\mu_f},\mathrm{Pr}=\frac{k_f\left(\rho Cp\right)_{nf}}{k_{nf}\left(\rho C_p\right)_f},Sc=\frac{k_f\left(\rho C_p\right)_{nf}}{D\left(\rho C_p\right)_f},u=\frac{v_r t^*}{r},r=\frac{r^*}{d},k_0=\frac{k_r^2\left(\rho C_p\right)_f}{\left(\rho C_p\right)_{nf}v^{*2}},$$

$$Gr_\theta=\frac{g\beta_{nf}(T-T_0)\mu_{nf}}{{v_r}^2\beta_f},Gr_c=\frac{g\beta_{nf}^*(C-C_0)\mu_{nf}}{{v_r}^2\beta_f^*},\theta=\frac{T-T_0}{T_0},C=\frac{C-C_0}{C_0},\Re=\frac{16\zeta T_0^3\rho_f}{3\alpha\left(C_p\right)_{nf}},$$

$$H_a=\frac{\sigma {B_0}^2 v_r}{\rho_{nf}},\sigma_0=\frac{\sigma_0}{v_r}$$

Transforming Equations (14), (15) and (16) in dimensionless form, the modelled equations can be expressed as

$$\frac{1}{r}\frac{\partial v_r}{\partial r}=\xi_1\frac{1}{\mathrm{Re}}\left[\frac{1}{r}\frac{\partial v_r}{\partial r}+\frac{\partial^2 v_r}{\partial r^2}\right]+\xi_2 Gr_\theta\theta+\xi_3 Gr_c C-\xi_4 H_a v_r-\xi_4\sigma_0 v_r \tag{25}$$

$$\frac{1}{r}\frac{\partial\theta}{\partial r}=\xi_5\frac{1}{\mathrm{Pr}}\left[\frac{1}{r}\frac{\partial\theta}{\partial r}+\frac{\partial^2\theta}{\partial r^2}\right]-\xi_6\Re\left(\frac{1}{r}\frac{\partial\theta}{\partial r}+\frac{\partial^2\theta}{\partial r^2}\right) \tag{26}$$

$$\frac{1}{r}\frac{\partial C}{\partial r}=\xi_6\frac{1}{Sc}\left[\frac{1}{r}\frac{\partial C}{\partial r}+\frac{\partial C^2}{\partial r^2}\right]-\xi_6\frac{1}{r}k_0 C \tag{27}$$

where (Re) is the Reynolds number, (Pr) is the Prandtl number, (Sc) is the Schmidt number, ($G_{r_\theta}\theta$,) is the thermal Grashof number, ($G_{r_c}C$) is the modified Grashof number, (R) is the thermal radiation parameter, (\theta) is the dimensionless temperature, (u) is the dimensionless velocity, (C) is the dimensionless concentration, (Ha) is the Hartmann number, (σ_0) denotes the electrical conductivity parameter, (k_0) is the dimensionless chemical reaction parameter, and (r) represents the dimensionless radial coordinate.

Furthermore, the effective dynamic viscosity ratio, effective thermal conductivity ratio, and other nondimensional thermo-physical properties of the silver nanofluid appearing in Equations (25) - (27) are expressed as follows:

$$\xi_1=\frac{\left\{1+2.5\phi_{np}+\left[3.125+\left(2.5/\phi_{np(\max)}\right)\right]\phi_{np}^2+....\right\}\mu_{bf}+\left(1+2.5\phi_{np}+2.5\phi_{np}^2+....\right)\mu_{bf}}{\left(1-\phi\right)+\phi\frac{\rho_s}{\rho_f}}$$

$$\xi_2=(1-\phi)+\phi\frac{\beta_s}{\beta_f}$$

$$\xi_3 = (1-\phi) + \phi \frac{\beta_s^*}{\beta_f^*}$$

$$\xi_4 = \frac{1}{(1-\phi) + \phi \frac{\rho_s}{\rho_f}}$$

$$\xi_5 = \frac{K_{bf}(1-\phi) + K_{np}\phi + 3C \frac{d_{bf}}{d_{np}} K_{bf} \, \mathrm{Re}_{d_{np}}^2 \, \mathrm{Pr}\,\phi + K_{bf} \frac{1-\phi+2\phi \frac{K_{np}}{K_{np}-K_{bf}} In \frac{K_{np}+K_{bf}}{2K_{bf}}}{1-\phi+2\phi \frac{K_{bf}}{K_{np}-K_{bf}} In \frac{K_{np}+K_{bf}}{2K_{bf}}}}{(1-\phi) + \phi \frac{(C_p)_s}{(C_p)_f}}$$

$$\xi_6 = \frac{1}{(1-\phi) + \phi \frac{(C_p)_s}{(C_p)_f}}$$

Table 2. *Numerical values of the nondimensional thermo-physical parameters employed in the present computations.*

Material Parameters/Properties	**Computational Values (K^{-1})**
Thermal expansivity of water (β_{bf})	2.1×10^{-4}
Thermal expansion due to temperature of nanofluid (β_{nf})	18.8×10^{-6}
Concentration expansivity of water $(\beta_{bf}{}^*)$	0.26
Concentration expansivity of silver $(\beta_{nf}{}^*)$	0.06
Diffusivity of water	2.23×10^{-6}
Stefan - Boltzmann constant (k_B)	1.38×10^{-23}

Equations (25) - (27) can be written as

$$\frac{\xi_1}{\mathrm{Re}} \frac{1}{r} \frac{\partial v_r}{\partial r} - \frac{1}{r} \frac{\partial v_r}{\partial r} + \frac{\xi_1}{\mathrm{Re}} \frac{\partial^2 v_r}{\partial r^2} + \xi_2 Gr_\theta \theta + \xi_3 Gr_c C - \xi_4 H_a v_r - \xi_4 \sigma_0 v_r = 0 \tag{28}$$

$$\frac{\xi_5}{\mathrm{Pr}} \frac{1}{r} \frac{\partial \theta}{\partial r} - \frac{1}{r} \frac{\partial \theta}{\partial r} + \frac{\xi_5}{\mathrm{Pr}} \frac{\partial^2 \theta}{\partial r^2} - \xi_6 \Re \frac{1}{r} \frac{\partial \theta}{\partial r} + \xi_6 \Re \frac{\partial^2 \theta}{\partial r^2} = 0 \tag{29}$$

$$\frac{\xi_6}{Sc} \frac{1}{r} \frac{\partial C}{\partial r} - \frac{1}{r} \frac{\partial C}{\partial r} + \frac{\xi_6}{Sc} \frac{\partial C^2}{\partial r^2} - \xi_6 \frac{1}{r} k_0 C = 0 \tag{30}$$

4. Method of Solution

The transformed governing equations, Equations (28) - (30), are solved analytically using the Laplace transform technique. Applying the Laplace transform to the governing equations yields

$$\frac{\xi_6}{Sc}(s\overline{C}(s)-C(0))-(s\overline{C}(s)-C(0))+\frac{\xi_6}{Sc}\frac{1}{s^2}(s^2\overline{C}(s)-sC(0)-C^1(0))-\xi_6 k_0\overline{C}(s)=0 \quad (31)$$

$$\frac{\xi_5}{\Pr}(s\overline{\theta}(s)-\theta(0))-(s\overline{\theta}(s)-\theta(0))+\frac{\xi_5}{\Pr}\frac{1}{s^2}(s^2\overline{\theta}(s)-s\theta(0)-\theta^1(0))-\xi_6\Re(s\overline{\theta}(s)-\theta(0))+\xi_6\Re\frac{1}{s^2}(s^2\overline{\theta}(s)-s\theta(0)-\theta^1(0))=0 \quad (32)$$

$$\begin{aligned}&\frac{\xi_1}{\mathrm{Re}}(s\overline{v}(s)-v(0))-(s\overline{v}(s)-v(0))+\frac{\xi_1}{\mathrm{Re}}\frac{1}{s^2}(s^2\overline{v}(s)-sv(0)-v^1(0))+\xi_2\frac{1}{s^2}Gr_\theta\overline{\theta}\\&+\xi_3\frac{1}{s^2}Gr_c\overline{C}-\xi_4\frac{1}{s^2}H_a\overline{v}(s)-\xi_4\frac{1}{s^2}\sigma_0\overline{v}(s)=0\end{aligned} \quad (33)$$

Applying the modified boundary conditions

$$\begin{aligned}&c(0)=1\\&c^1(0)=0\end{aligned} \quad (34)$$

$$\begin{aligned}&\theta(0)=1\\&\theta^1(0)=0\end{aligned} \quad (35)$$

$$\begin{aligned}&v(0)=1\\&v^1(0)=0\end{aligned} \quad (36)$$

The inverse Laplace transform is subsequently employed to recover the physical solutions in the spatial domain and with subject to the modified boundary conditions Equations (31), (32) and (33) becomes

$$\overline{C}(s)=\frac{\frac{\xi_6}{Sc}\frac{1}{s}+\frac{\xi_6}{Sc}-1}{\frac{\xi_6}{Sc}s+\frac{\xi_6}{Sc}-\xi_6 k_0-s} \quad (37)$$

$$\overline{\theta}(s)=\frac{\frac{\xi_5}{\Pr}+\frac{\xi_5}{\Pr}\frac{1}{s}+\xi_6\Re\frac{1}{s}-\xi_6\Re-1}{\frac{\xi_5}{\Pr}s+\frac{\xi_5}{\Pr}+\xi_6\Re-\xi_6\Re s-s} \quad (38)$$

$$\overline{v}(s)=\frac{\frac{\xi_1}{\mathrm{Re}}\frac{1}{s}+\frac{\xi_1}{\mathrm{Re}}-\xi_2\frac{1}{s^2}Gr_\theta\left(\frac{\frac{\xi_5}{\Pr}+\frac{\xi_5}{\Pr}\frac{1}{s}+\xi_6\Re\frac{1}{s}-\xi_6\Re-1}{\frac{\xi_5}{\Pr}s+\frac{\xi_5}{\Pr}+\xi_6\Re-\xi_6\Re s-s}\right)-\xi_3\frac{1}{s^2}Gr_c\left(\frac{\frac{\xi_6}{Sc}\frac{1}{s}+\frac{\xi_6}{Sc}-1}{\frac{\xi_6}{Sc}s+\frac{\xi_6}{Sc}-\xi_6 k_0-s}\right)-1}{\frac{\xi_1}{\mathrm{Re}}s+\frac{\xi_1}{\mathrm{Re}}-s-\xi_4\frac{1}{s^2}H_a-\xi_4\frac{1}{s^2}\sigma_0} \quad (39)$$

5. Engineering Application

The present study combines the effective thermal conductivity models proposed by Jang and Choi and Xue together with the effective viscosity correlations of Mooney and Saito to provide a comprehensive representation of the thermophysical behaviour of silver nanofluids. The combined thermal conductivity model accounts for the influence of Brownian motion, nanoparticle concentration, particle size, temperature, and particle geometry, while the viscosity model improves the prediction of momentum transport, pressure distribution, and flow resistance. These models have important engineering applications in the design and optimization of electronic cooling systems, compact heat exchangers, microchannel heat sinks, nuclear reactor cooling systems, chemical processing equipment, solar thermal collectors, and advanced thermal management technologies, where accurate prediction of heat transfer and fluid flow is essential.

The wall shear stress is characterized by the skin friction coefficient, which quantifies the frictional resistance between the flowing silver nanofluid and the cylindrical surface. The skin friction coefficient is evaluated from the velocity distribution given by Equation (39) as

$$\tau=\left.\frac{dv(r)}{dr}\right|_{r=0} \quad (40)$$

Under identical circumstances, the Nusselt number is the ratio of heat transmission by convection to heat transfer via fluid conduction. The Nusselt number measures the balance between convective and conductive heat transfer at a fluid's boundary, as it pertains to fluid dynamics. The dimensionless group known as the Nusselt number (Nu) is essential in the fields of fluid mechanics and heat transport. It successfully connects the dots between a system's thermal conductivity, characteristic length, and convective heat transfer coefficient. In this way, we may get the Nusselt number by solving Equation (38).

$$Nu=-\left.\frac{d\theta(r)}{dr}\right|_{r=0} \quad (41)$$

Similarly, the mass transfer characteristics are described by the Sherwood number, which represents the ratio of convective to diffusive mass transfer. The local Sherwood number is obtained from the concentration distribution in Equation (37) as

$$Sh = -\left.\frac{dC(r)}{dr}\right|_{r=0} \tag{42}$$

6. Results and Discussions

The influence of the governing dimensionless parameters on the thermal energy transport characteristics of magnetohydrodynamic silver nanofluid flow over a cylindrical geometry is analysed using the analytical solutions obtained from Eqs. (37) - (39). The inverse Laplace transform is employed to evaluate the velocity, temperature, and concentration distributions under the prescribed boundary conditions. The effects of the Reynolds number, Prandtl number, Schmidt number, Hartmann number, thermal Grashof number, modified Grashof number, thermal radiation parameter, and chemical reaction parameter on the flow and thermal fields are illustrated in Figures 1-8 and Tables 3-15. Particular attention is devoted to their influence on the velocity profile, temperature distribution, concentration profile, skin friction coefficient, Nusselt number, and Sherwood number. The numerical results provide valuable insight into the thermal transport behaviour of silver nanofluids and their potential application in advanced engineering thermal management systems.

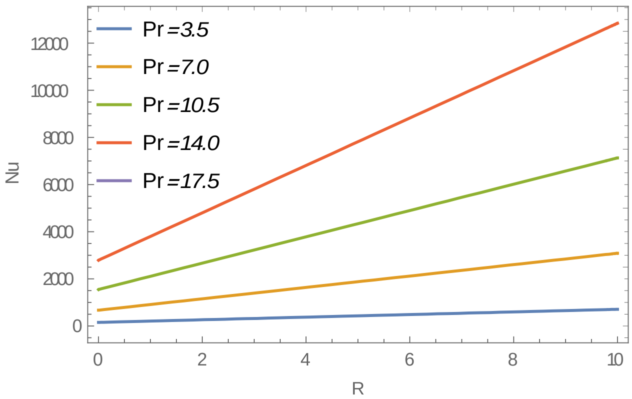

Figure 1. *Nusselt number (Nu) against boundary layer of Radiation (R) with Prandtl number (Pr) varying.*

Figure 1 illustrates the variation of the Nusselt number with the thermal radiation parameter for different values of the Prandtl number. It is observed that increasing the Prandtl number enhances the Nusselt number, indicating an improvement in the convective heat transfer rate at the cylindrical surface. This behaviour is attributed to the reduction in thermal boundary-layer thickness associated with higher Prandtl numbers, which promotes steeper temperature gradients at the wall. Consequently, the combined thermal conductivity model predicts more efficient thermal energy transport within the silver nanofluid.

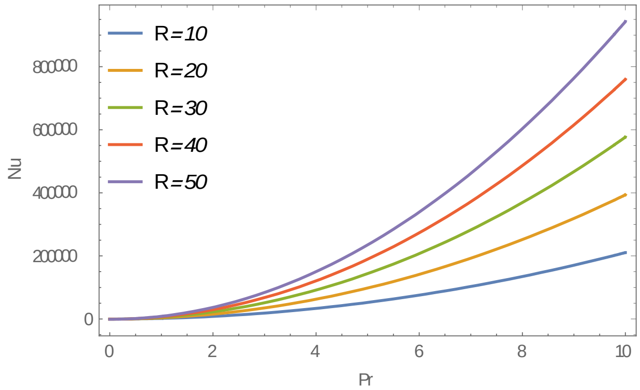

Figure 2. *Nusselt number (Nu) against boundary layer of Prandtl number (Pr) with Radiation (R) varying.*

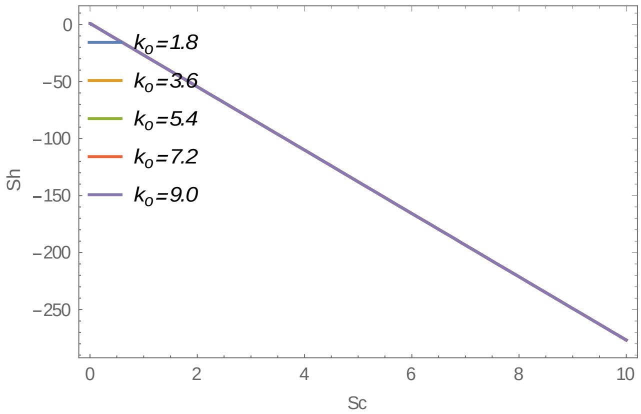

Figure 3. *Sherwood number (Sh) against boundary layer of Schmidt number (Sc) with Chemical reaction (K_0) term varying.*

Figure 2 presents the influence of the thermal radiation parameter on the Nusselt number for different Prandtl numbers. The results show that increasing the radiation parameter leads to a gradual reduction in the Nusselt number. This trend suggests that thermal radiation weakens the temperature gradient at the cylinder surface, thereby reducing the rate of convective heat transfer. The observation demonstrates that radiative heat transfer modifies the overall thermal energy transport characteristics of the magnetohydrodynamic silver nanofluid.

Figure 3 depicts the variation of the Sherwood number with the Schmidt number for different values of the chemical reaction parameter. The Sherwood number represents the ratio of convective mass transfer to molecular diffusion. It is observed that increasing the chemical reaction parameter reduces the Sherwood number, indicating a decrease in mass transfer at the cylindrical surface. This behaviour results from the consumption of diffusing species through chemical reactions, which suppresses concentration gradients within the boundary layer.

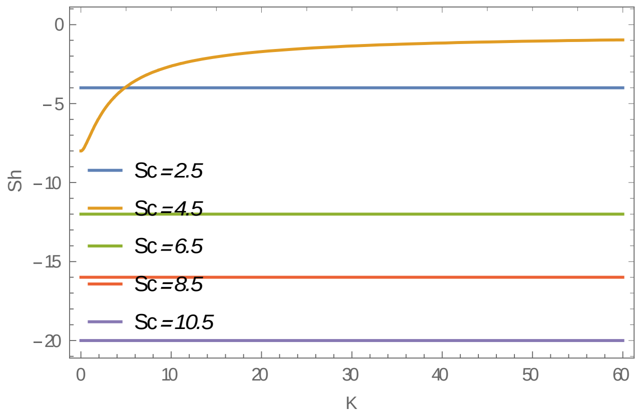

Figure 4. *Sherwood number (Sh) against boundary layer of Chemical reaction (K_0) with Schmidt number (Sc) varying*

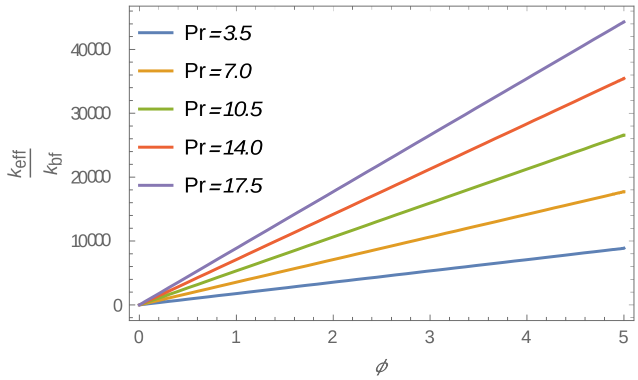

Figure 5. *Jang and Choi (2004) model of thermal conductivity ratio against nanoparticle volume fraction (φ) for varying Prandtl number (Pr) with K_{np} = 0.01, C = 2.3, Re = 10.*

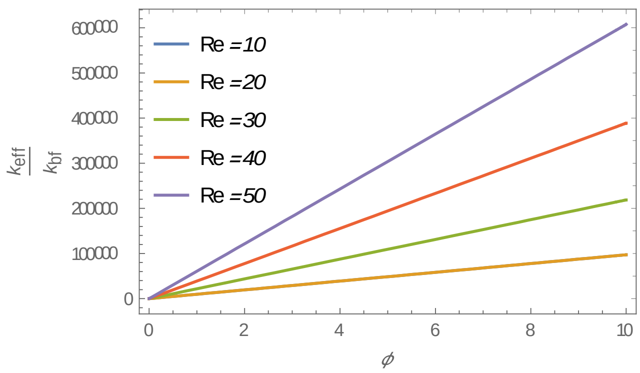

Figure 6. *Jang and Choi (2004) model of thermal conductivity ratio against nanoparticle volume fraction (φ) for varying Reynolds number (Re) with K_{np} = 0.01, C = 2.3, Pr = 3.5.*

Figure 4 shows the variation of the Sherwood number with the chemical reaction parameter for different Schmidt numbers. The results indicate that increasing either the Schmidt number or the chemical reaction parameter enhances the Sherwood number. Higher Schmidt numbers correspond to lower molecular diffusivity, producing steeper concentration gradients near the wall and consequently increasing the rate of mass transfer from the cylindrical surface.

Figure 5 illustrates the variation of the effective thermal conductivity ratio with nanoparticle volume fraction for different Prandtl numbers. The effective thermal conductivity increases with increasing nanoparticle volume fraction, confirming that the addition of silver nanoparticles substantially improves the thermal transport capability of the base fluid. Furthermore, fluids with lower Prandtl numbers exhibit relatively higher effective thermal conductivity because thermal diffusion dominates momentum diffusion, leading to thicker thermal boundary layers and enhanced heat transport.

Figure 6 presents the effect of the Reynolds number on the effective thermal conductivity ratio as the nanoparticle volume fraction varies. It is evident that increasing the Reynolds number slightly reduces the effective thermal conductivity ratio. This behaviour is associated with increased inertial effects, which alter nanoparticle dispersion within the base fluid. The observed trend is consistent with Brownian motion theory, where continuous particle interactions, collisions, and agglomeration influence the effective thermo-physical properties of the silver nanofluid.

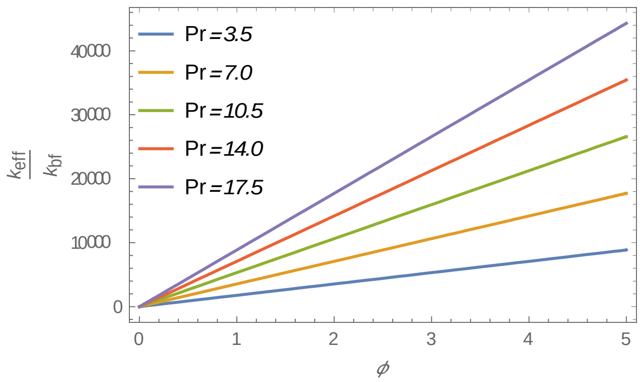

Figure 7. *Jang and Choi (2004) and Xue (2005) models of thermal conductivity ratio against nanoparticle volume fraction (φ) for varying Prandtl number (Pr) with K_{np} = 0.01, C = 2.3, Re = 10.*

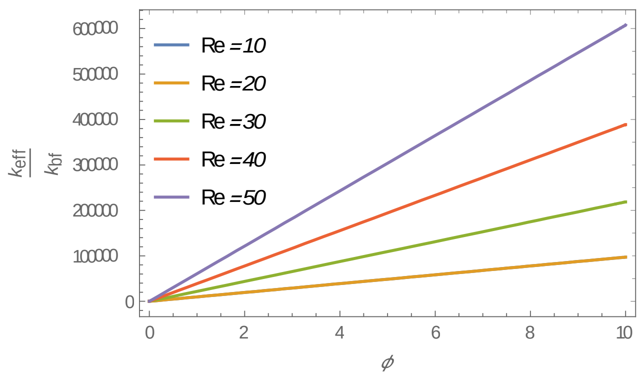

Figure 8. *Jang and Choi (2004) and Xue (2005) models of thermal conductivity ratio against nanoparticle volume fraction (φ) for varying Reynolds number (Re) with K_{np} = 0.02, C = 2.3, Pr = 3.5.*

Figure 7 illustrates the predictions of the combined thermal conductivity models for different Prandtl numbers. The results indicate that increasing the Prandtl number decreases the effective thermal conductivity ratio for a given nanoparticle volume fraction. This reduction is attributed to the diminished thermal diffusivity associated with larger Prandtl numbers, resulting in lower thermal energy transport through the nanofluid.

Figure 8 presents the influence of the Reynolds number on the combined thermal conductivity model. The effective thermal conductivity ratio decreases slightly as the Reynolds number increases, reflecting the transition of the silver nanofluid from a predominantly diffusion-controlled regime toward stronger inertial flow. Under magnetohydrodynamic conditions, this transition modifies the interaction between the applied magnetic field and the conducting silver nanofluid, thereby influencing the overall thermal transport characteristics. The observed behaviour is consistent with previously reported studies on MHD nanofluid heat transfer [31].

7. Numerical Computation of Nusselt Number, Sherwood Number, Skin Friction

Table 3. *Nusselt number varying Prandtl number.*

	Nusselt number parameters values used, R = 3.5 and $\varphi = 0.02$
Pr	Nu
3.5	2.42424
7.0	2.81535
10.5	3.50650
14.0	4.34987
17.5	5.39366

Table 4. *Nusselt number varying Radiation term.*

	Nusselt number parameters values used, Pr = 3.5 and $\varphi = 0.02$
R	Nu
3.5	2.42424
6.5	2.57388
9.5	2.72353
12.5	2.87317
15.5	3.02282

Table 5. *Sherwood number varying Schmidt number.*

	Sherwood number parameters values used, k_0= 1.8, and $\varphi = 0.02$
Sc	Sh
2.5	2.24186
4.5	2.81535
6.5	3.50652
8.5	4.34987
10.5	5.39366

Table 6. *Sherwood number varying Chemical reaction term.*

	Sherwood number parameters values used, Sc = 2.5, and $\varphi = 0.02$
k_0	Sh
1.8	-0.45513
3.6	-0.44746
5.4	-0.43286
7.2	-0.42345
9.0	-0.41123

Table 7. *Skin friction varying Chemical reaction term.*

	Skin friction parameters values used, Re = 10, Pr = 3.5, Sc = 2.5, $Gr_\theta = 2.6$, Gr_c= 3.2, R =3.5, Ha = 0.5, σ = 0.25 and $\varphi = 0.02$
k_0	τ
1.8	-111.234781
3.6	-109.123580
5.4	-107.112477
7.2	-104.102145
9.0	-101.088823

Table 8. *Skin friction varying Grashof number due to temperature.*

	Skin friction parameters values used, Re = 10, Pr = 3.5, Sc = 2.5, $Gr_c = 3.2$, R =3.5, k_0= 1.8, Ha = 0.5, σ = 0.25 and $\varphi = 0.02$
Gr_θ	τ
2.6	-126.330456166566

	Skin friction parameters values used, Re = 10, Pr = 3.5, Sc = 2.5, $Gr_c = 3.2$, R =3.5, k_0= 1.8, Ha = 0.5, σ = 0.25 and $\varphi = 0.02$
5.2	-366.330456166776
7.8	-446.341456166447
10.4	-562.430456166223
13.0	-636.323456166122

Table 9. Skin friction varying Grashof number due to concentration.

	Skin friction parameters values used, Re = 10, Pr = 3.5, Sc = 2.5, $Gr_\theta = 2.6$, R =3.5, k_0= 1.8, Ha = 0.5, σ = 0.25 and $\varphi = 0.02$
Gr_c	τ
3.2	-126.3104001166566
6.5	-366.3004112166776
9.5	-446.3111226166447
12.5	-562.3321456166211
16.5	-636.2234156166122

Table 10. Skin friction varying Prandtl number.

	Skin friction parameters values used, Re = 10, Sc = 2.5, $Gr_\theta = 2.6$, $Gr_c = 3.2$, R =3.5, k_0= 1.8, Ha = 0.5, σ = 0.25 and $\varphi = 0.02$
Pr	τ
3.5	122.2104001166522
7.0	266.3004112166733
10.5	346.3111226155522
14.0	461.33210216166211
17.5	534.22341561660231

Table 11. Skin friction varying Schmidt number.

	Skin friction parameters values used, Re = 10, Pr = 3.5, Sc = 2.5, $Gr_\theta = 2.6$, $Gr_c = 3.2$, R =3.5, k_0= 1.8, Ha = 0.5, σ = 0.25 and $\varphi = 0.02$
Sc	τ
2.5	-111.114781
4.5	-109.113580
6.5	-107.102477
8.5	-104.092145
10.5	-101.088811

Table 12. Skin friction varying Radiation term.

	Skin friction parameters values used, Re = 10, Pr = 3.5, Sc = 2.5, $Gr_\theta = 2.6$, $Gr_c = 3.2$, R =3.5, k_0= 1.8, Ha = 0.5, σ = 0.25 and $\varphi = 0.02$
R	τ
3.5	122.2104221166112
6.5	266.2204112145433
9.5	346.3444122615552
12.5	461.32320216166211
15.5	534.45761561660231

Table 13. Skin friction varying Magnetic Hartmann number.

	Skin friction parameters values used, Re = 10, Pr = 3.5, Sc = 2.5, $Gr_\theta = 2.6$, $Gr_c = 3.2$, R =3.5, k_0= 1.8, σ = 0.25 and $\varphi = 0.02$
Ha	τ
0.5	-126.1224001166566
1.5	-115.3241121667763
2.5	-104.2611226166447
3.5	-102.3321456234111
4.5	-101.2234155446234

Table 14. Skin friction varying Electroconductivity parameter.

	Skin friction parameters values used, Re = 10, Pr = 3.5, Sc = 2.5, $Gr_\theta = 2.6$, $Gr_c = 3.2$, R =3.5, k_0= 1.8, Ha = 0.5, and $\varphi = 0.02$
σ	τ
0.25	-103.1004001166566
0.50	-102.2111121667763
0.75	-101.1101226166447
1.00	-100.1001456234111
1.25	-100.1000155446101

Table 15. *Skin friction varying Reynolds number.*

Skin friction parameters values used, Pr = 5.5, Sc =1.8, $Gr_\theta = 2.6$, $Gr_c = 3.2$, R =3.5, k_0= 1.6, Ha = 1.35, σ = 0.25 and $\varphi = 0.02$

Re	τ
10	-126.21110011665663
20	-223.12001121667761
30	-336.10112261664472
40	-443.21314561662112
50	-556.13134156166122

Table 3 presents the variation of the Nusselt number with the Prandtl number. The numerical results indicate that the Nusselt number increases monotonically from 2.42424 to 5.39366 as the Prandtl number increases from 3.5 to 17.5. This behaviour demonstrates that larger Prandtl numbers enhance convective heat transfer at the cylindrical surface by reducing thermal diffusivity and producing steeper temperature gradients within the thermal boundary layer.

Table 4 illustrates the influence of the thermal radiation parameter on the Nusselt number. The results reveal that the Nusselt number increases gradually with increasing radiation parameter, indicating that thermal radiation contributes positively to heat transfer in the present model. This enhancement is attributed to the additional thermal energy supplied by radiative heat transfer, which increases the wall temperature gradient and consequently improves the convective heat transfer rate.

Table 5 shows the variation of the Sherwood number with the Schmidt number. It is observed that increasing the Schmidt number increases the Sherwood number significantly. Since larger Schmidt numbers correspond to lower mass diffusivity, steeper concentration gradients develop near the cylinder surface, thereby enhancing the convective mass transfer rate.

Table 6 presents the effect of the chemical reaction parameter on the Sherwood number. Although the Sherwood number remains negative throughout the investigated range, its magnitude decreases as the chemical reaction parameter increases. This trend suggests that stronger chemical reactions reduce concentration gradients within the boundary layer, thereby weakening the overall mass transfer process.

Table 7 illustrates the variation of the skin friction coefficient with the chemical reaction parameter. The results show that increasing the chemical reaction parameter reduces the magnitude of the skin friction coefficient, indicating a gradual reduction in wall shear stress due to the modification of the concentration boundary layer by chemical reactions.

Table 8 presents the effect of the thermal Grashof number on the skin friction coefficient. As the thermal Grashof number increases, the magnitude of the skin friction coefficient increases considerably. This behaviour indicates that thermal buoyancy forces strengthen the fluid motion near the cylindrical surface, thereby increasing the wall shear stress.

Table 9 shows the influence of the concentration Grashof number on the skin friction coefficient. Similar to the thermal Grashof number, increasing the concentration Grashof number increases the magnitude of the skin friction coefficient owing to stronger buoyancy effects arising from concentration differences within the nanofluid.

Table 10 presents the effect of the Prandtl number on the skin friction coefficient. The numerical results indicate that the skin friction coefficient increases with increasing Prandtl number. This behaviour is associated with the reduction in thermal diffusivity, which strengthens the velocity gradient near the cylinder wall and consequently increases the wall shear stress.

Table 11 illustrates the influence of the Schmidt number on the skin friction coefficient. Increasing the Schmidt number reduces the magnitude of the skin friction coefficient, indicating that lower molecular diffusivity weakens the wall shear stress under the present flow conditions.

Table 12 shows the variation of the skin friction coefficient with the thermal radiation parameter. The numerical results indicate that the skin friction coefficient increases with increasing radiation parameter. This behaviour demonstrates that thermal radiation enhances momentum transport within the boundary layer, resulting in greater wall shear stress.

Table 13 presents the effect of the Hartmann number on the skin friction coefficient. As the Hartmann number increases, the magnitude of the skin friction coefficient decreases. The applied magnetic field generates a Lorentz force that suppresses fluid motion, thereby reducing wall shear stress and stabilizing the flow.

Table 14 illustrates the influence of the electrical conductivity parameter on the skin friction coefficient. Increasing the electrical conductivity parameter decreases the magnitude of the skin friction coefficient. The enhanced interaction between the conducting silver nanofluid and the applied magnetic field strengthens the electromagnetic damping effect, thereby reducing wall shear stress.

Table 15 shows the effect of the Reynolds number on the skin friction coefficient. The numerical results indicate that the magnitude of the skin friction coefficient increases steadily with increasing Reynolds number. This behaviour reflects the growing influence of inertial forces within the flow, leading to larger velocity gradients and higher wall shear stress at the cylindrical surface.

8. Conclusions

A parametric assessment of thermal energy transport in magnetohydrodynamic silver nanofluid flow over a cylindrical geometry has been presented by combining the effective thermal conductivity models of Jang and Choi (2004) and Xue (2005) with the effective viscosity correlations of Mooney

(1951) and Saito (1950). The governing equations were formulated in cylindrical coordinates and solved analytically using the Laplace transform method.

The principal findings of the present investigation are summarized as follows:

1) Increasing the Prandtl number significantly enhances the Nusselt number, indicating improved convincing heat transfer due to thinner thermal boundary layers.
2) Thermal radiation contributes positively to heat transfer by increasing the Nusselt number, demonstrating its beneficial role in enhancing thermal energy transport in silver nanofluids.
3) The Sherwood number increases with increasing Schmidt number, whereas stronger chemical reactions reduce its magnitude, indicating suppression of mass transfer through species consumption.
4) The magnitude of the skin friction coefficient increases with increasing thermal and concentration Grashof numbers, Prandtl number, thermal radiation parameter, and Reynolds number, reflecting enhanced momentum transport near the cylindrical surface.
5) Increasing the Hartmann number and electrical conductivity parameter reduces the magnitude of the skin friction coefficient owing to the damping effect of the Lorentz force generated by the applied magnetic field.
6) The combined thermal conductivity and viscosity models provide a more comprehensive representation of the thermo-physical behaviour of silver nanofluids by simultaneously accounting for Brownian motion, nanoparticle concentration, particle geometry, particle size, and viscosity effects.
7) The analytical model developed in this study provides valuable theoretical insight for the design and optimization of advanced thermal management systems employing electrically conducting silver nanofluids in applications such as electronic cooling, heat exchangers, chemical reactors, microchannel heat sinks, and energy conversion systems operating under magnetic field environments.

Abbreviations

MHD	Magnetohydrodynamics
Ag	Silver
Re	Reynolds Number
Pr	Prandtl Number
Sc	Schmidt Number
Ha	Hartmann Number
Nu	Nusselt Number
Sh	Sherwood Number
Gr	Grashof Number
M	Magnetic Parameter
CFD	Computational Fluid Dynamics
DOI	Digital Object Identifier
LTT	Laplace Transform Technique

Author Contributions

Ojo Adetoye Solomon: Conceptualization, Data curation, Formal Analysis, Investigation, Methodology, Software, Validation, Visualization, Writing – original draft, Writing – review & editing

Nwabuzor Peter Onyelukachukwu: Conceptualization, Methodology, Project administration, Supervision, Validation, Resources, Writing – original draft, Writing – review & editing

Conflicts of Interest

The authors declare no conflicts of interest.

References

[1] Choi, S. U. S. (1995). Enhancing thermal conductivity of fluids with nanoparticles. In D. A. Siginer & H. P. Wang (Eds.), *Developments and Applications of Non-Newtonian Flows* (ASME FED, Vol. 231, pp. 99-105). American Society of Mechanical Engineers.

[2] Gardner, R. A., Uherka, K. L., & Lykoudis, P. S. (1966). Influence of a transverse magnetic field on forced convection liquid-metal heat transfer. *AIAA Journal, 4*(5), 848-852.

[3] Zakariya, M., Maher, M., Khalid, N., & Regis, D. (2012). Heat transfer in magnetohydrodynamic fluid flows: A review. *Research Journal of Applied Sciences, Engineering and Technology, 4*(15), 2412-2421.

[4] Das, S. K., Choi, S. U. S., & Patel, H. E. (2006). Heat transfer in nanofluids—A review. *Heat Transfer Engineering, 27*(10), 3-19.

[5] Huang, C. C., & Lin, T. F. (1995). Vortex flow and thermal characteristics in mixed convection of air in a horizontal rectangular duct: Effects of the Reynolds and Grashof numbers. *International Journal of Heat and Mass Transfer, 38*(9), 1661-1674.

[6] Yih, K. A. (1999). MHD forced convection flow adjacent to a non-isothermal wedge. *International Communications in Heat and Mass Transfer, 26*(6), 819-827.

[7] Gowda, R. P. J., Kumar, R. N., Khan, U., Prasannakumara, B. C., Zaib, A., Ishak, A., & Galal, A. M. (2022). Dynamics of nanoparticle diameter and interfacial layer on flow of non-Newtonian (Jeffrey) nanofluid over a convective curved stretching sheet. *International Journal of Modern Physics B, 36*(31), 2250224.

[8] Bühler, L. (2007). Magnetohydrodynamic flows in liquid metal blankets and related heat transfer problems. *Fusion Engineering and Design, 82*(15-24), 2895-2903.

[9] Wang, X. Q., & Mujumdar, A. S. (2007). Heat transfer characteristics of nanofluids: A review. *International Journal of Thermal Sciences, 46*(1), 1-19.

[10] Zniber, K., Oubarra, A., & Lahjomri, J. (2005). Analytical solution to the problem of heat transfer in an MHD flow inside a channel with prescribed sinusoidal wall heat flux. *Energy Conversion and Management, 46*(7-8), 1147-1163.

[11] João, A. L., João, N. N. Q., & Emanuel, N. M. (2007). Integral transform analysis of MHD flow and heat transfer in parallel-plate channels. *International Communications in Heat and Mass Transfer, 34*(3), 420-431.

[12] Yamamoto, Y., Kunugi, T., Satake, S., & Smolentsev, S. (2008). DNS and k-model simulation of MHD turbulent channel flows with heat transfer. *Fusion Engineering and Design, 83*(7-9), 1309-1312.

[13] Oztop, H. F., & Abu-Nada, E. (2008). Numerical study of natural convection in partially heated rectangular enclosures filled with nanofluids. *International Journal of Heat and Fluid Flow, 29*(5), 1326-1336. https://doi.org/10.1016/j.ijheatfluidflow.2008.04.009

[14] Lo, D. C. (2010). High-resolution simulations of magnetohydrodynamic free convection in an enclosure with a transverse magnetic field using a velocity-vorticity formulation. *International Communications in Heat and Mass Transfer, 37*(8), 514-523.

[15] Kakaç, S., & Pramuanjaroenkij, A. (2009). Review of convective heat transfer enhancement with nanofluids. *International Journal of Heat and Mass Transfer, 52*(13-14), 3187-3196.

[16] Takahashi, M., Aritomi, M., Inoue, A., & Matsuzaki, M. (1998). MHD pressure drop and heat transfer of lithium single-phase flow in a rectangular channel under a transverse magnetic field. *Fusion Engineering and Design, 42*(1-4), 365-372.

[17] Mahian, O., Kianifar, A., Kalogirou, S. A., Pop, I., & Wongwises, S. (2013). A review of the applications of nanofluids in solar energy. *International Journal of Heat and Mass Transfer, 57*, 582-594.

[18] Tiwari, R. K., & Das, M. K. (2007). Heat transfer augmentation in a two-sided lid-driven differentially heated square cavity utilizing nanofluids. *International Journal of Heat and Mass Transfer, 50*(9-10), 2002-2018. https://doi.org/10.1016/j.ijheatmasstransfer.2006.09.034

[19] Buongiorno, J. (2006). Convective transport in nanofluids. Journal of Heat Transfer, 128(3), 240-250. https://doi.org/10.1115/1.2150834

[20] Adetoye S. O., Peter O. N., Chijioke A. E., and Edikan S. U. (2026). The Application of Homotopy Perturbation Method in Newtonian Fluids. *Fluid Mechanics.* 11(1), pp. 1-11.

[21] A. S. Ojo, A. T. Ngiangia, M. C. Onyeaju. (2025). Comparative effects of energy transfer on silver nanofluid in magnetohydrodynamic flow via the cylindrical surface”. Journal of Nanofluids. Vol. 14, pp, 1-11, 2025.

[22] Adetoye S, O., Alalibo, N., Onyeaju M., and Chijioke A, E. (2025). Energy transfer on magnetohydrodynamic silver nanofluid flow past a cylindrical enclosure. Journal of Nanofluid, Vol. 14, pp. 639-648.

[23] Gaslter, K. K., Bariska, L. T., and Astral, T. A. (2011). Theory of Hartmann profile and application. *International Journal of Mathematical analysis.* 45(56), pp. 267-301.

[24] A. S. Ojo, A. T. Ngiangia, M. C. Onyeaju. (2025). Numerical analysis of energy transfer on magnetohydrodynamic silver nanofluid flow in cylindrical coordinate. Open Journal of Physical Sci ence. Vol 6, pp, 63-82, 2025.

[25] Mintsa, H. G., Roy, C., Nguyen, M and Doucet E. (2009)**.** New temperature dependent thermal conductivity data for water-based nanofluids. *Int. J. Therm. Sci*. 48(2), pp. 363-371.

[26] Jang, S. P., & Choi, S. U. S. (2004). Role of Brownian motion in the enhanced thermal conductivity of nanofluids. *Applied Physics Letters, 84*(21), 4316-4318. https://doi.org/10.1063/1.1756684

[27] Xue, Q. (2005). Model for effective thermal conductivity of nanofluids. *Physics Letters A, 344*(2-4), 371-379. https://doi.org/10.1016/j.physleta.2005.07.061

[28] Mooney, M. (1951). The viscosity of a concentrated suspension of spherical particles. *Journal of Colloid Science, 6*(2), 162-170.

[29] Saito, N. (1950). Concentration dependence of the viscosity of high polymer solutions. *Journal of the Physical Society of Japan, 5*(1), 4-8.

[30] Ngiangia, A. T., and Nwabuzor, P. O., (2016). Convective heat flux characteristics of MHD fluid with oscillatory suction and variable electroconductivity over a vertical plate provoked by radiation. *Asian Journal of Physical Sciences.* 1(2), pp. 1-18.

[31] Cogley, A. C., Vincent, W. G. and Gilles, S. E., (1968)**.** Differential approximation to radiation heat transfer in a non-grey gas near equilibrium. *The American Institute of Aeronautic and Aetronautics.* 6(4), pp. 551-553.